Geological sulfur isotopes indicate elevated OCS in the Archean atmosphere, solving faint young sun paradox

Yuichiro Ueno[a,b], Matthew S. Johnson[c,1], Sebastian O. Danielache[b,c,d], Carsten Eskebjerg[c], Antra Pandey[b,d], and Naohiro Yoshida[b,d,e]

[a]Global Edge Institute and [b]Research Center for the Evolving Earth and Planet, Tokyo Institute of Technology, Meguro Tokyo, 152-8551, Japan; [c]Copenhagen Center for Atmospheric Research, Department of Chemistry, University of Copenhagen, Universitetsparken 5 DK-2100 Copenhagen Ø, Denmark; and [d]Departments of Environmental Science and Technology and [e]Environmental Chemistry and Engineering, Tokyo Institute of Technology, G1-25, 4259 Nagatsuta, Yokohama, 226-8502, Japan

Edited by Mark H. Thiemens, University of California at San Diego, La Jolla, CA, and approved July 14, 2009 (received for review March 31, 2009)

Distributions of sulfur isotopes in geological samples would provide a record of atmospheric composition if the mechanism producing the isotope effects could be described quantitatively. We determined the UV absorption spectra of $^{32}SO_2$, $^{33}SO_2$, and $^{34}SO_2$ and use them to interpret the geological record. The calculated isotopic fractionation factors for SO_2 photolysis give mass independent distributions that are highly sensitive to the atmospheric concentrations of O_2, O_3, CO_2, H_2O, CS_2, NH_3, N_2O, H_2S, OCS, and SO_2 itself. Various UV-shielding scenarios are considered and we conclude that the negative $\Delta^{33}S$ observed in the Archean sulfate deposits can only be explained by OCS shielding. Of relevant Archean gases, OCS has the unique ability to prevent SO_2 photolysis by sunlight at $\lambda > 202$ nm. Scenarios run using a photochemical box model show that ppm levels of OCS will accumulate in a CO-rich, reducing Archean atmosphere. The radiative forcing, due to this level of OCS, is able to resolve the faint young sun paradox. Further, the decline of atmospheric OCS may have caused the late Archean glaciation.

mass independent fractionation | carbonyl sulfide (OCS) | sulfur dioxide (SO_2) | photochemistry | greenhouse gases

Mass independent fractionation (MIF) of sulfur isotopes has been found in geological samples older than 2.3 billion years (Ga) and is believed to be produced by the photochemical reactions of gaseous sulfur compounds in a low-oxygen reducing atmosphere (1–4). The rise of atmospheric oxygen (O_2 and O_3) would have oxidized atmospheric sulfur compounds to sulfate, preventing the accumulation of isotopic fractionation in two reservoirs. Moreover, it would have blocked UV sunlight inhibiting the supposed photochemical process(es) producing the isotope anomaly. In contrast, given reducing conditions, two isotopically distinct sulfur species such as elemental sulfur (polysulfur) and sulfate could be formed photochemically and precipitate at the surface, where the MIF signal could be preserved in sediment (3–5). Sulfur MIF in geological samples is regarded as indicating an anoxic atmosphere.

This assertion relies on assumptions as to the origin of the MIF, although the mechanisms are still poorly known. Broad agreement in the $\Delta^{36}S/\Delta^{33}S$ ratio (≈ -1) in pre-2.3 Ga sedimentary rocks (1, 6, 7) and those produced in the laboratory by SO_2 photolysis suggest that photodissociation of gas-phase SO_2 most likely accounts for MIF in the Archean (2). Indeed, SO_2 photolysis is a key rate limiting step, particularly in a low-O_2 reducing atmosphere (4, 8). In addition, two mechanisms have been proposed whereby sulfur MIF could be formed under oxidizing conditions in the modern atmosphere: (*i*) Photolysis of SO_3 at altitudes greater than $\approx$50 km, where reaction between SO_3 and H_2O is slow, is claimed to be responsible for the MIF found in modern stratospheric aerosol (8). In contrast, at lower altitudes, SO from SO_2 photolysis reforms SO_2, so fractionation in SO_2 photolysis would not affect the isotopic composition of aerosol (8, 9). (*ii*) In extreme volcanic events resulting in highly elevated atmospheric SO_2 concentrations, SO_2 photoexcitation below the dissociation threshold at 220 nm generates electronically excited SO_2^* that reacts with SO_2 to form SO and SO_3, which is assumed to produce MIF (9). The resulting SO_3 combines with water to form sulfuric acid and may carry the MIF signal. Under low-oxygen conditions, SO_2 photolysis is the prime candidate for producing Archean MIF (8).

Despite mechanisms that can explain production and preservation of MIF in aerosols, no previous model can reproduce the multiple isotope composition of photochemically produced sulfate aerosol. Archean sulfate deposits show uniformly negative $\Delta^{33}S$ values (1, 7, 10), which have been claimed to match laboratory studies of SO_2 photolysis at 193 nm (2). However, the solar spectrum is a broad continuum, not a sharp laser wavelength. Photolysis using a sun-like continuum (high pressure Xe lamp) yields positive $\Delta^{33}S$ values of product sulfate (2), which is incompatible with the geological record. To resolve the apparent discrepancy, it is necessary to understand the wavelength dependence of the mass independent isotope effect. Recent theoretical studies have examined the UV absorption spectra of SO_2 isotopologues (11) and have suggested that SO_2 self-shielding may have caused the Archean MIF record (12). However, the theoretical spectra necessarily contain several approximations and do not agree with recently obtained isotopologue-specific experimental spectra (13). The most straightforward way to determine the MIF effect is via direct measurement of UV absorption by SO_2 isotopologues.

In a recent article, we presented the absorption spectra of three SO_2 isotopologues from 190 to 330 nm (13). Based on these spectra, we present here the multiple isotope fractionation factors for SO_2 photolysis as a function of wavelength. Further, we predict the $\Delta^{33}S$ value of sulfate aerosols under several atmospheric UV-shielding scenarios and present a new interpretation of Archean atmospheric chemistry, which can explain the geological record of MIF. This approach is similar to our earlier experimental work with N_2O, which was used in the isotopic analysis of the Anthropocene atmosphere (14).

Results

Wavelength-Dependent Isotope Effect of SO_2 Photolysis. Fig. 1 shows the spectra of the fractionation and mass independent anomaly

Author contributions: Y.U., M.S.J., and N.Y. designed research; S.O.D. and C.E. performed research; M.S.J. and N.Y. contributed new reagents/analytic tools; Y.U., M.S.J., S.O.D., and A.P. analyzed data; and Y.U., M.S.J., and S.O.D. wrote the paper.

The authors declare no conflict of interest.

This article is a PNAS Direct Submission.

[1]To whom correspondence should be addressed. E-mail: msj@kiku.dk.

This article contains supporting information online at www.pnas.org/cgi/content/full/0903518106/DCSupplemental.

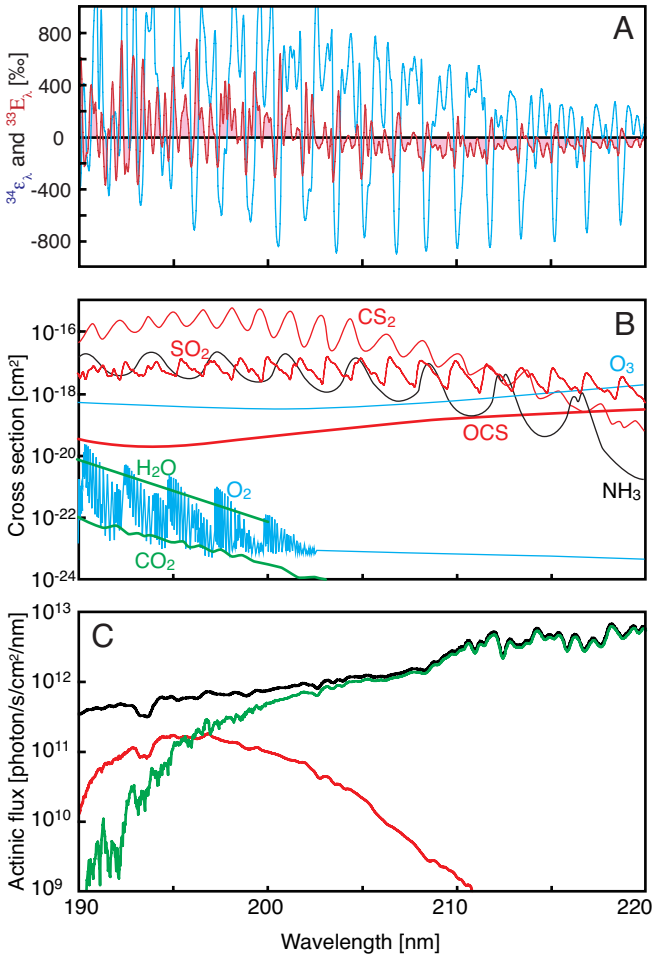

Fig. 1. UV spectra of isotopic fractionation factors, absorption by atmospheric molecules and actinic flux. (*A*) Wavelength-dependent photolysis fractionation and three-isotope constants recalculated from high-precision absorption spectra of SO_2 isotopologues (13). The blue and red lines represent $^{34}S/^{32}S$ fractionation ($^{34}\varepsilon_\lambda$) and the deviation from a mass-dependent relationship ($^{33}E_\lambda$), respectively. Note that SO_2 photolysis above and below 202 nm gives generally negative and positive $^{33}E_\lambda$, values, respectively. The definition of $^{33}E_\lambda$ is different from that found in ref. 13. (*B*) The absorption spectra of the UV-shielding molecules. (*C*) Present-day solar spectrum (black; see ref. 36) and attenuated actinic flux calculated at 10-km altitude in the model Archean Atmospheres 1 (green) and 3 (red).

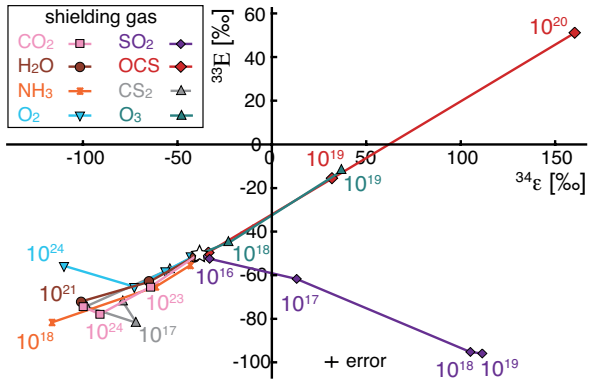

Fig. 2. Process-dependent two- and three-isotope fractionations from SO_2 photolysis calculated for different columns of each shielding gas. The number adjacent to each point shows the overhead column of shielding gas (molecules/cm²). Points are spaced at one log unit intervals. Calculations were terminated when opacity became <0.01. The star shows result for solar UV spectrum without atmospheric attenuation.

factors. There is a significant wavelength-dependent mass independent isotope effect due to the red-shifting of peak locations and changes in the profiles of the vibronic absorption features (Fig. 1 and Fig. S1) (13). Averaged over several nanometers, the mass independent isotope effect $^{33}E_\lambda$ is generally negative at $\lambda > 202$ nm, and positive for $\lambda < 202$ nm (Fig. 1*A*). This broad trend is the most important factor determining isotopic fractionation by SO_2 photolysis under a variety of atmospheric scenarios. Because different atmospheric molecules attenuate different regions of the solar actinic flux spectrum (Fig. 1 *B* and *C*), the magnitude and sign of the isotope effects in SO_2 photolysis will be sensitive to the chemical composition of the atmosphere. The primary aim of this study is to estimate fractionation factors and multiple isotope effects as a function of the overhead column of a number of key UV and VUV-shielding molecules.

Effect of Atmospheric UV Shielding on Isotopic Fractionation of SO_2 Photolysis. The two- and three-isotope fractionation factor spectra can be used to calculate process fractionation constants for photolysis in a given atmospheric scenario (15). The values of $^{34}\varepsilon$ [$= 1{,}000(^{34}J/^{32}J - 1)$] and ^{33}E [$= 1{,}000(^{33}J/^{32}J - (^{34}J/^{32}J)^{0.515})$] are based on the isotopologues' photolysis rates J, which are sensitive to the concentrations of UV-shielding molecules in the atmosphere. We consider CO_2, H_2O, O_2, O_3, NH_3, CS_2, OCS, and SO_2, which possess significant absorption cross-sections in the wavelength region of the SO_2 photodissociation band (190–220 nm). These few molecules are part of a greater number of 490 atmospherically relevant molecules that were investigated (*SI Text*).

Fig. 2 shows the resulting isotope effects of SO_2 photolysis. The isotope effects for different shieldings intersect at $\approx^{34}\varepsilon = -39‰$ and $^{33}E = -51‰$. This region represents photolysis in an atmosphere with negligibly small opacity. When the column density increases, three types of behavior are seen. First, an increase in CO_2, H_2O, NH_3, CS_2, or O_2 concentration produces a similar negative shift of $^{34}\varepsilon$ and ^{33}E (Fig. 2), because these gases generally attenuate wavelengths shorter than 202 nm (Fig. 1). In contrast, O_3 and OCS shielding shift $^{34}\varepsilon$ and ^{33}E toward more positive values because they attenuate wavelengths longer than 202 nm. In contrast, an increase of O_3 or OCS has the opposite effect. Finally, SO_2 self-shielding produces increasing $^{34}\varepsilon$ and decreasing ^{33}E. The previous estimate of isotope effects in SO_2 photolysis from self-shielding found an increasing trend in ^{33}E (12) that is opposite to our result. The reason for the difference may be because the spectra of the isotopically substituted species were approximated by shifting the absorption peaks of the natural abundance SO_2 spectrum using a set of isotope-dependent frequency shifts. These shifts were based on vibrational wavefunctions calculated using a single ab initio SO_2 excited potential energy surface (11, 12). However, SO_2 has a score of electronic states in the relevant energy region with multiple curve crossings, giving rise to the complicated pattern seen in the experimental results (13). For example, three vibronic peaks of the three isotopologues are found between 200 and 205 nm (Fig. S1). First $^{33}SO_2$, then $^{34}SO_2$, and then $^{32}SO_2$ has the highest peak intensity. Whereas the isotopologues' peak positions shift linearly with distance from the band origin, the peak intensities, widths, and profiles of the vibrational structure change in a complex "mass independent" manner. A theoretical description of the origin of these isotope effects awaits further study.

An important conclusion from the model is that the mass-independent isotope effect ^{33}E for SO_2 photolysis shows a negative sign for most UV-shielding scenarios (Fig. 2). In these

GEOPHYSICS

cases, sulfate aerosol would acquire a positive $\Delta^{33}S$ value. This value is because sulfate would be produced by oxidation of residual SO_2 in the photochemical reaction network (4, 5) (Fig. S2). The predicted positive $\Delta^{33}S$ of the sulfate is incompatible with the geological record suggesting Archean seawater sulfate would have had negative $\Delta^{33}S$ values (1, 3, 7, 10). This apparent discrepancy could be resolved if the Archean atmosphere contained an appreciable amount of O_3 or OCS. Of molecules commonly found in terrestrial atmospheres, only these two selectively shield the λ>202 nm region, yielding the opposite direction of mass independent isotope effect ^{33}E (Fig. 1 and *SI Text*). However, for these molecules the required overhead column to produce a positive ^{33}E is $>10^{19}$ molecule/cm^2. Such an ozone column is comparable with that of the present day O_2-rich atmosphere, and thus unlikely to have explained Archean MIF, because it would have prevented the preservation of MIF itself. Therefore, we examine the possibility of an OCS-shielding scenario using an atmospheric chemical reaction model. Previous model studies of the Archean atmosphere have not included OCS chemistry, although OCS may have been the dominant sulfur species in a reducing atmosphere. At >500 ppt, OCS is the most abundant sulfur species in today's atmosphere, in part because the UV cross section of OCS is an order of magnitude smaller than other gaseous sulfur species like SO_2, CS_2 and H_2S (Fig. 1*B*). Moreover, if the atmosphere were anoxic and rich in CO, such high levels of OCS could have been produced by reactions of CO with polysulfur (16, 17).

Atmospheric Reaction Model. To predict the isotopic composition of sulfate aerosols, we performed a numerical simulation using fractionation factors for SO_2 photolysis calculated for different atmospheric scenarios (Figs. S2–S5 and Tables S1–S3). We introduced OCS photochemistry into the model, which was not included in the previous models of Archean atmosphere (3–5, 18). The model calculation gives the concentrations of various sulfur compounds and the isotopic composition of product sulfate and elemental sulfur aerosols at a given time after injecting 10 ppm of SO_2 into the model atmosphere. We show here the results of the simulation assuming three model atmospheres (Table S1): (*i*) 1% CO_2 ($CO/CO_2 = 0.1$), (*ii*) 1% CO ($CO/CO_2 = 10$), and (*iii*) 5 ppm OCS ($CO/CO_2 = 10$). All of the models assume total pressure (N_2) of 1 bar at surface and a low O_2 level (10^{-12} PAL).

Under high-CO_2 conditions (Atmosphere 1), 99.9% of injected SO_2 is converted into sulfate within the first day (Fig. S4). In this case, MIF (i.e., non-zero $\Delta^{33}S$) in sulfate aerosol cannot occur, because all sulfur entering the atmosphere is deposited as sulfate (Figs. S4 and S5). Even if the atmosphere contains virtually no molecular oxygen (O_2: 10^{-12} PAL), the oxidation capacity of the CO_2-rich atmosphere ($CO/CO_2 < 1$) is high enough to prevent the formation of reduced-form sulfur compounds including elemental sulfur aerosol. Such an oxidizing atmosphere (i.e., high CO_2) cannot explain the Archean MIF record. Our model is too simple to determine the precise threshold of CO_2 necessary to erase MIF, but low CO_2 conditions are qualitatively necessary to preserve sulfur MIF. Also, our model results, including OCS chemistry, strengthen the theory that low atmospheric O_2 levels ($<10^{-5}$ PAL) are required to explain the Archean MIF record (4).

Subseqently, for a CO-rich more-reducing scenario (Atmosphere 2), we found that 90% of injected SO_2 is converted into OCS within the first day and most of the remaining 10% is transformed into sulfate (Fig. S4). After the accumulation of OCS, elemental sulfur (S_8) forms slowly (10^8 molecules/cm^3/hour) from OCS. In this case, sulfate aerosol acquires a large positive $\Delta^{33}S$ (Figs. S4 and S5) that is isotopically balanced by a negative $\Delta^{33}S$ pool of reduced sulfur. As suggested (2–5), the reducing atmosphere allows formation of two reservoirs allowing preservation of atmospheric MIF in aerosols. The resulting positive $\Delta^{33}S$ value of sulfate is again inconsistent with the geological record. However, the estimated isotopic composition of the atmospheric sulfur species largely depends on the fractionation factors for SO_2 photolysis, which are changed by the atmospheric UV-shielding scenario. In Atmosphere 2, OCS is not added to the overhead column, although our calculations demonstrate that OCS can accumulate in such a CO-rich reducing atmosphere because OCS production ($S + CO + M \rightarrow OCS + M$) is faster than OCS photolysis and S_x forming reactions ($S_x + OCS \rightarrow S_{x+1} + CO$). Assuming the slow production of S_8 is the main sink of OCS, a sulfur influx of 6×10^{11} mole/year is required to sustain 1 ppm OCS (or 1.6×10^{14} mole in the entire atmosphere). This influx is only 3× larger than the modern volcanic outgassing rate (2×10^{11} mole/year) (19). Hence, it is not unlikely that an OCS level high enough to modify the UV field could have been maintained, especially during periods of high volcanic activity.

Finally, we examined Atmosphere 3, in which 5 ppm of OCS was added into the previous CO-rich Atmosphere 2. The resulting concentrations of sulfur species after injection of SO_2 are similar to those of Atmosphere 2, although their isotopic compositions are different. In contrast to Atmosphere 2, sulfate aerosol acquires a negative $\Delta^{33}S$ because overhead OCS attenuates the 202–220 nm region (Figs. 1, 2, and Fig. S4). The OCS-rich reducing atmosphere is consistent with the negative $\Delta^{33}S$ signature of Archean marine sulfate deposits (1, 3, 7, 10). Based on previous geological investigations, photochemical fractionations in the Archean atmosphere exhibited positive correlations between $\delta^{34}S$ and $\Delta^{33}S$ with a slope of 0.6–0.8 (Fig. 3). This trend is approximately similar to that of the OCS-rich atmosphere (Fig. 3), although this positive correlation between $\delta^{34}S$ and $\Delta^{33}S$ is only preliminary and does not necessarily match the geological observation in this present stage, because the model assumes no isotopic fractionation other than SO_2 photolysis. Most other reactions are likely characterized by mass dependent fractionation, which does not change $\Delta^{33}S$ (only $\delta^{34}S$) values, and some photolysis reactions may cause mass independent fractionation, which can change both $\Delta^{33}S$ and $\delta^{34}S$ values. Nonetheless, the assumption that isotopic fractionation only occurs by SO_2 photolysis is valid for predicting the $\Delta^{33}S$ values of aerosol species, because it is the key rate-limiting step particularly under reducing conditions (Fig. S2). To test this assumption, we performed additional simulations, assuming that the same magnitude ($^{34}\varepsilon$ = 40‰), but opposite sign of MIF, occurs by SO, SO_3, H_2S, and OCS photolysis reactions and by SO_2 photoexcitation in addition to MIF by SO_2 photolysis. These models all yield practically the same result as the model, assuming that MIF only occurs by SO_2 photolysis. Hence, acquisition of a negative $\Delta^{33}S$ in sulfate aerosol is a plausible scenario in an OCS-rich reducing atmosphere. However, mineral sulfide could have been derived from elemental sulfur reduction and from sulfate reduction, biologically or abiologically (3), thus acquiring both positive and negative $\Delta^{33}S$.

In summary, our atmospheric reaction models show that sulfate aerosol acquires a MIF signature when the atmosphere is reducing ($CO/CO_2 > 1$), whereas a more oxidizing atmosphere does not allow preservation of MIF due to the quantitative conversion of sulfur into sulfate. SO_2 photolysis is the most important reaction controlling the isotopic composition of sulfate aerosols, which mainly reflects that of residual SO_2 after the photolysis. These conclusions are consistent with previous model studies without OCS chemistry (3–5). In the reducing atmosphere, however, sulfur entering the atmosphere would be largely converted into OCS. This conversion implies that high OCS levels (>1 ppm) would be expected if the atmosphere is rich in CO (>1%), and the volcanic sulfur flux was >3× larger than the modern volcanic outgassing rate. In this case, due to the

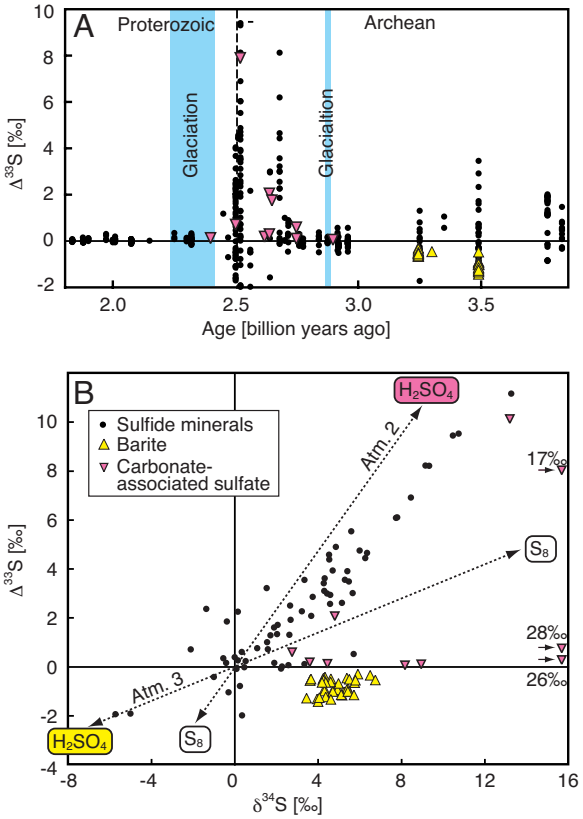

Fig. 3. Geological sulfur isotope distributions. (*A*) Secular variations of the $\Delta^{33}S$ values of sedimentary sulfide (black) and sulfate (yellow). The isotopic composition of trace sulfate replacing carbonate lattice are also shown (red). The data are from refs. 6, 7, 28, and references therein. (*B*) The $\delta^{34}S$ and $\Delta^{33}S$ relationship of the Archean (>2.5 Ga) deposits compared with our models results. Dashed lines labeled as Atm. 2 and 3 show the trends of product sulfate and sulfur aerosols in the model Atmospheres 2 and 3.

unique UV-shielding effect of OCS, sulfate would have acquired a negative $\Delta^{33}S$ value as observed in Archean deposits. However, in a period of lower volcanic activity, the aerosol sulfate may have also possessed MIF, but with a positive $\Delta^{33}S$ value.

Implications for the Archean Atmosphere. Our study demonstrates that an OCS-rich reducing atmosphere would not only preserve MIF but also explain the negative $\Delta^{33}S$ value in sulfate from Archean deposits older than 3 Ga (Fig. 3). We propose that the early to middle Archean atmosphere would have contained ppm levels of OCS.

Such a high level of OCS would have been associated with significant radiative forcing, because OCS absorbs in the infrared window region from 8–13 μm, where heat energy would normally escape to space. Overall, OCS at 10 ppm would have had a radiative forcing of $\approx$60 W/m^2, approximately the same as that of 1% CO_2 or 100 ppm of CH_4. Hence, ppm-level OCS would have played a significant role for maintaining a warm climate for the early Earth.

Despite the prediction of models of solar evolution that the Archean Sun would have been 20–30% less bright than today, geological evidence suggests that the Archean Earth was warm enough that the ocean was not completely frozen (the faint young Sun paradox; see ref. 20). This relative warmth implies the Archean atmosphere may have contained more greenhouse gas than the present atmosphere. An alternative explanation, considering the sun's mass loss history, is that the early sun was brighter than has previously been thought, although the period of mass loss is likely shorter than what is required to resolve the paradox (21). Greenhouse gases that have been suggested include NH_3 (20, 22), CO_2 (18, 23), and CH_4 (4, 5, 24).

A CO_2 mixing ratio of >30% would have been required to compensate a 30% decrease in solar luminosity (18). Such a high CO_2 concentration is, however, incompatible with the preservation of sulfur MIF, because a high CO_2 Atmosphere 1 (1% CO_2) would suppress the MIF signature, as noted above. In addition, geochemical studies of late Archean paleosols indicate CO_2 levels of <1% (25, 26). Although Archean CO_2 (<1%) may have been higher than today, greenhouse warming by CO_2 alone is unable to resolve the paradox (27).

Ammonia has the potential to be the most effective greenhouse gas, because the absorption band of NH_3 almost entirely covers the IR window (8–13 μm) (20). However, greenhouse warming by NH_3 is now considered to be unlikely because it would be photolyzed rapidly (18, 27). In contrast, Sagan and Chyba (22) argued that the hydrocarbon haze generated by methane photolysis may have shielded the UV flux, and thus allowed $\approx$1 ppm NH_3 in the Archean atmosphere, which is sufficient to maintain a surface temperature above freezing. However, UV-shielding by a hydrocarbon haze is problematic because it would have cooled the planet (27). This dilemma may be partly solved by considering UV-shielding by OCS. Given the UV-flux of Atmosphere 3, the photolysis rate of NH_3 under 1 to 10 ppm OCS would have been 1 to 2 orders of magnitude lower than without OCS. Hence, shielding by ppm levels of OCS may have allowed a higher NH_3 level than previously thought, although the shielding would not have been perfect (Fig. 1), thus indirect radiative forcing by OCS via enhanced NH_3 should also be considered in a reducing Archean atmosphere.

Greenhouse warming by CH_4 is favored by several authors (5, 24–28). More than 100 ppm of CH_4 may have been reached if the atmosphere was reducing, and if active biological CH_4 production is assumed (24, 27, 29). Previous model calculations indicate that 1,000-ppm CH_4 alone is not enough, but the combined effects of CO_2 and CH_4 may have compensated the low solar flux (27). Although the OCS-rich reducing atmosphere does not conflict with this scenario, our results suggest that a high CH_4 level of >100 ppm may not have been necessary given an OCS level of >10 ppm. In addition, the OCS bending overtone at $\approx$9.5 μm does not overlap with CO_2 or CH_4, giving OCS a relatively high global warming potential. Thus, OCS would have acted as a potent greenhouse gas even when large amounts of CO_2 and CH_4 were present in the atmosphere.

Given an important warming role for OCS in the Archean, the decline of OCS is likely to have caused Precambrian glaciations, particularly at $\approx$2.9 Ga (Pongola glaciation; see ref. 30). It has been known that the magnitude of the MIF decreased at approximately this time, followed by an increase (Fig. 3). A tentative O_2-rise at $\approx$2.9 Ga has been proposed (31), but is now thought to be unlikely due to a small but clear MIF signature in many sulfide deposits (32, 33). The $\Delta^{33}S$ value of seawater sulfate after the Pongola glaciation is still poorly understood, although recent analysis of carbonate-associated sulfate (28) suggests that the late Archean sulfate may have possessed the opposite sign of $\Delta^{33}S$ anomaly in contrast to those of early to middle Archean (Fig. 3). The decline of OCS would result in a change of ^{33}E in SO_2 photolysis (Fig. 2) and thus may explain the change of $\Delta^{33}S$ of sulfate from negative through zero to a possibly positive sign.

The atmospheric models presented here are an initial attempt at predicting the $\Delta^{33}S$ value of aerosol sulfate for a set of atmospheric shielding scenarios. Further model studies are needed to evaluate the relative contributions of the greenhouse gases. Nonetheless, a CO-rich reducing atmosphere would have resulted in OCS-rich conditions when volcanic sulfur input was high enough. Moreover, such an atmosphere is so far the only one that can explain both the preservation of MIF and the

negative $\Delta^{33}S$ values of Archean sulfate deposits. Hence, UV-shielding and the greenhouse effect of OCS should be considered for any model of the Archean atmosphere. These results are qualitative and remain to be confirmed by more advanced models of the Archean atmosphere and further laboratory studies.

Methods

Definitions of Wavelength-Dependent Isotope Effects ($^{34}\varepsilon_\lambda$ and $^{33}E_\lambda$). Wavelength dependent isotope effects for SO_2 photolysis can be calculated from the following equations (15):

$$^{33}\epsilon_\lambda = 1000(^{33}\sigma_\lambda/^{32}\sigma_\lambda - 1)\ ^0/_{00} \quad [1]$$

$$^{34}\epsilon_\lambda = 1000(^{34}\sigma_\lambda/^{32}\sigma_\lambda - 1)\ ^0/_{00} \quad [2]$$

where $^{32}\sigma_\lambda$, $^{33}\sigma_\lambda$, and $^{34}\sigma_\lambda$ represent absorption cross sections of $^{32}SO_2$, $^{33}SO_2$, and $^{34}SO_2$, respectively, at wavelength λ [nm] (13). Deviation from mass-dependent fractionation is described using:

$$^{33}E_\lambda = {}^{33}\epsilon_\lambda - 1000\ ((1 + {}^{34}\epsilon_\lambda/1000^{0.515} - 1)\ ^0/_{00} \quad [3]$$

Note that $^{33}\varepsilon_\lambda$, $^{34}\varepsilon_\lambda$, and $^{33}E_\lambda$ are functions of wavelength and are different from the process dependent isotope effects ($^{34}\varepsilon$ and ^{33}E), resulting from UV radiation under a specific set of atmospheric or experimental conditions.

Definitions of Process-Dependent Isotope Effects ($^{34}\varepsilon$ and ^{33}E). The isotopic fractionation factor is defined as the ratio of the reaction rate of the minor to the major isotopic species. For SO_2 photolysis, the fractionation factors are defined as:

$$^{33}\alpha = {}^{33}J/{}^{32}J \quad [4]$$

$$^{34}\alpha = {}^{34}J/{}^{32}J \quad [5]$$

where ^{32}J, ^{33}J, and ^{34}J are photolysis rates of $^{32}SO_2$, $^{33}SO_2$, and $^{34}SO_2$, respectively. In general, isotope effects are expressed in units of parts per thousand (‰):

$$^{33}\epsilon = 1000(^{33}\alpha - 1)\ ^0/_{00} \quad [6]$$

$$^{34}\epsilon = 1000(^{34}\alpha - 1)\ ^0/_{00} \quad [7]$$

The mass dependent relationship describing the equilibrium distribution of three sulfur isotopes between phases has been established by (34):

$$^{33}\alpha = {}^{34}\alpha^{0.515} \quad [8]$$

Using Eqs. **6**, **7**, and **8**, deviation from the mass dependent relationship is described as:

$$^{33}E = {}^{33}\epsilon - 1000[(1 + {}^{34}\epsilon/1000)^{0.515} - 1] \approx {}^{33}\epsilon - 0.515{}^{34}\epsilon\ ^0/_{00} \quad [9]$$

The approximation applies to near-mass dependent conditions.

Photolysis Rates of SO_2 Isotopologues and Change of the Isotope Effect Due to Atmospheric UV Shielding. The actual isotopic fractionation factors $^{33}\alpha$ (= $^{33}J/^{32}J$; see Eq. **4**) and $^{34}\alpha$ (= $^{34}J/^{32}J$; see Eq. **5**) can be estimated from the photolysis rate J of the relevant SO_2 isotopologue. The J values at different atmospheric conditions can be calculated from absorption cross sections (13):

$$J = \int_{190}^{220} \varphi(\lambda)\sigma(\lambda)I(\lambda)e^{-\tau(\lambda)}d\lambda \quad [10]$$

where $\varphi(\lambda)$ is the photodissociation quantum yield, $\sigma(\lambda)$ is the absorption cross section of each SO_2 isotopologue, $I(\lambda)$ is the solar spectrum at the top of the atmosphere and $\tau(\lambda)$ is the opacity term of the overhead column of absorbing species. We are concerned with the effect of isotopic substitution on J and will describe here the values taken for $\varphi(\lambda)$, $I(\lambda)$ and $\tau(\lambda)$.

Quantum Yield $\varphi(\lambda)$. The photodissociation quantum yield was estimated using:

$$\varphi(\lambda) = 1 - \varphi_f(\lambda) \quad [11]$$

where $\varphi_f(\lambda)$ is fluorescence quantum yield. The estimated $\varphi(\lambda)$ is practically unity at wavelengths shorter than 210 nm and drops to zero at 220 nm, which represents the energetic threshold for breaking the bond (35). Hence, we neglect wavelengths longer than 220 nm in calculating J (Eq. **10**). The used $\varphi(\lambda)$ was obtained by fitting the experimental data of relative fluorescence quantum yields published by Okazaki et al. (35). We applied the same $\varphi(\lambda)$ value for the three isotopologues.

Solar Spectrum I(λ). The modern solar actinic flux is used in Eq. **10**. The spectrum is taken from the SOLSTICE project's results from the Upper Atmosphere Research Satellite (36). The Archean solar UV spectrum may have been different, although the expected change in solar UV emission through time is unlikely to affect our estimate (*SI Text*).

Atmospheric Composition τ(λ). The opacity term contained in Eq. **10** has been calculated as

$$\tau(\lambda) = \sum_i \sigma_i(\lambda) \int \rho_i(z)dz \quad [12]$$

where $\sigma_i(\lambda)$ is the absorption cross section of UV shielding molecule i and $\int\rho_i(z)dz$ is the overhead column density of molecule i above an altitude z. The gases defining the opacity term in this work have significant cross sections in the 190–220-nm wavelength range (i.e., CO_2, H_2O, O_2, O_3, NH_3, CS_2, OCS, and SO_2). The thickness of the overhead column (in molecules/cm^2) is determined by the UV light absorbing properties of each molecule and is calculated separately for each case. To evaluate isotopic fractionation given UV shielding (Fig. 2), we calculate Eq. **10** only when the transparency term $e^{-\tau(\lambda)}$ was from 0.01 to 0.99. When $e^{-\tau(\lambda)} < 0.01$, SO_2 is not photolyzed, whereas when $e^{-\tau(\lambda)} > 0.99$, the shielding effect is negligibly small. Details are given in *SI Text*.

Atmospheric Reaction Model. Numerical simulations (cf. Fig. S2) were performed to predict the isotopic composition of sulfate aerosol, using the calculated fractionation factors for SO_2 photolysis as a function of the overhead column of UV-shielding molecules.

The vertical profile of atmospheric species is prescribed for calculating photolysis rates at a given altitude in the model atmospheres. We examined three model atmospheres (Table S1). Although the chemical composition of the Archean atmosphere is largely unknown, our Atmosphere 2 assumed 1 bar total pressure (mainly N_2) at surface with 1% CO, 0.1% CO_2, 100 ppm H_2, and 10^{-12} PAL O_2. This composition and vertical profile mimic the ''standard Archean atmosphere'' used by Pavlov et al. (27). Model Atmosphere 1 assumes higher CO_2 (1% CO_2 and 0.1% CO), and Atmosphere 3 includes 5 ppm OCS in addition to Atmosphere 2. For all models, nitrogen, methane, and hydrocarbon chemistries were neglected for simplicity, although the redox state is critical for sulfur photochemistry. In our model, the redox state is controlled by changing the CO/CO_2 ratio at a constant H_2 level.

The simulation gives concentrations of atmospheric sulfur species and their isotopic compositions as a function of time after injecting 10 ppm SO_2. This injection simulates volcanic SO_2 input into the atmosphere. H_2S was neglected because the H_2S/SO_2 ratio is only 0.02 when assuming a typical redox buffer of magma.

The scenario photochemistries were modeled using KINTECUS (v3.8; www.kintecus.com). Our model includes 123 reactions (Tables S2 and S3). The rate constants of these reactions generally follow those used in refs. 4 and 27 and the OCS chemistries used in ref. 17. The aerosol species (S_8 and H_2SO_4) are assumed not to react further and to be removed quantitatively from the system, presumably by rainout or deposition. The vertical transport and mixing of atmospheric species was not considered.

To model isotopic fractionations, we considered sulfur isotopologues for the reactions involving sulfur chemistry. For instance, reactions R86a to R86i are the 9 subreactions generated using ^{32}S, ^{33}S, and ^{34}S in $S_2 + CO \rightarrow OCS + S$. Although not shown in the tables, the total number of reactions is 988, including the sulfur isotopic subreactions. In cases such as R86, the rates of the subreactions were determined assuming a statistical distribution of products. Our approach follows that of Pavlov and Kasting (4). Physical consistency of the model was checked by test runs assuming mass dependent fractionation in SO_2 photolysis (R1 in Table S2), which resulted in zero $\Delta^{33}S$ for product sulfur and sulfate aerosols.

In the model, no isotopic fractionation is assumed for any reactions except for SO_2 photolysis, for example, OCS photolysis is not associated with large isotopic

fractionation (37). This assumption is probably not correct, although SO_2 photolysis is often the rate limiting step for sulfate production in a reducing atmosphere, and hence likely controls the isotopic composition of aerosols (2–5). Sensitivity tests, adding the same magnitude but opposite sign of MIF effects to all of the other photolysis reactions (R2 to R11 in Table S2), give practically the same $\Delta^{33}S$ values of sulfate and sulfur aerosols when a reducing atmosphere is assumed (i.e., Atmospheres 2 and 3). This conclusion is consistent with previous model studies (2, 8, 12). Ono et al. (3) suggest SO photolysis may also affect the isotopic compositions of aerosol species, however, SO photolysis is faster than SO_2 and thus is not a key rate limiting step in our model.

ACKNOWLEDGMENTS. This work is supported by the 21st Century Center of Excellence Program ''How to build habitable planets,'' Tokyo Institute of Technology, sponsored by the Ministry of Education, Culture, Sports, Technology and Science, Japan (Y.U., S.O.D., and N.Y.), and by the Global Environment Research Fund (B-094) of the Ministry of the Environment, Japan. Y.U. is supported by MEXT's program ''Promotion of Environmental Improvement for Independence of Young Researchers'' under the Special Coordination Funds for Promoting Science and Technology and by KAKENHI (19740310). M.S.J, C.E., and S.D. thank the Copenhagen Center for Atmospheric Research supported by the Danish Natural Science Research Foundation and the Villum Kann Rasmussen Fund for its generous support.

1. Farquhar J, Bao H, Thiemens M (2000) Atmospheric influence of Earth's earliest sulfur cycle. *Science* 289:756–758.
2. Farquhar J, Savarino J, Airieau S, Thiemens MH (2001) Observation of wavelength-sensitive mass-independent sulfur isotope effects during SO_2 photolysis: Applications to the early atmosphere. *J Geophys Res* 12:32829–32839.
3. Ono S, et al. (2003) New insights into Archean sulfur cycle from mass-independent sulfur isotope records from the Hamersley Basin, Australia. *Earth Planet Sci Lett* 213:15–30.
4. Pavlov AA, Kasting JF (2002) Mass-independent fractionation of sulfur isotopes in Archean sediments: Strong evidence for an anoxic Archean atmosphere. *Astrobiology* 2:27–41.
5. Zahnle K, Claire M, Catling D (2007) The loss of mass-independent fractionation in sulfur due to a Palaeoproterozoic collapse of atmospheric methane. *Geobiology* 4:271–283.
6. Kaufman AJ, et al. (2007) Late Archean biospheric oxygenation and atmospheric evolution. *Science* 317:1900–1903.
7. Ueno Y, Ono S, Rumble D, Maruyama S (2008) Quadruple sulfur isotope analysis of ca. 3.5 Ga Dresser Formation: New evidence for microbial sulfate reduction in the Early Archean. *Geochim Cosmochim Acta* 72:5675–5691.
8. Pavlov AA, Mills MJ, Toon OB (2005) Mystery of the volcanic mass-independent sulfur isotope fractionation signature in the Antarctic ice core. *Geophys Res Lett* 32:L12816.
9. Savarino J, Romero A, Cole-Dai J, Bekki S, Thiemens MH (2003) UV induced mass-independent sulfur isotope fractionation in stratospheric volcanic sulfate. *Geophys Res Lett* 30:2131.
10. Bao H, Rumble D, Lowe DR (2007) The five stable isotope compositions of Fig Tree barites: Implications on sulfur cycle in ca. 3.2 Ga oceans. *Geochim Cosmochim Acta* 71:4868–4879.
11. Ran H, Xie D, Guo H (2007) Theoretical studies of C^1B_2 absorption spectra of SO_2 isotopomers. *Chem Phys Lett* 439:280–283.
12. Lyons JR (2007) Mass-independent fractionation of sulfur isotopes by isotope-selective photodissociation of SO_2. *Geophys Res Lett* 34:L22811.
13. Danielache SO, Eskebjerg C, Johnson MS, Ueno Y, Yoshida N (2008) High-precision spectroscopy of ^{32}S, ^{33}S and ^{34}S sulfur dioxide: Ultraviolet absorption cross sections and isotope effects. *J Geophys Res* 113:D17314.
14. von Hessberg P, et al. (2004) Ultra-violet absorption cross sections of isotopically substituted nitrous oxide species: $^{14}N^{14}NO$, $^{15}N^{14}NO$, $^{14}N^{15}NO$, and $^{15}N^{15}NO$. *Atmos Chem Phys* 4:1237–1253.
15. Grage MML, Nyman G, Johnson MS (2006) HCl and DCl: A case study of different approaches for determining photo fractionation constants. *Phys Chem Chem Phys* 8:4798–4804.
16. Yung YL, et al. (2009) Evidence for carbonyl sulfide (OCS) conversion to CO in the lower atmosphere of Venus. *J Geophys Res* 114:E00B34.
17. Krasnopolsky VA (2007) Chemical kinetic model for the lower atmosphere of Venus. *Icarus* 191:25–37.
18. Kasting JF (1982) Stability of ammonia in the primitive terrestrial atmosphere. *J Geophys Res* 87:3091–3098.
19. Bluth GJ, Schnetzler CC, Krueger AJ, Walter LS (1993) The contribution of explosive volcanism to global atmospheric sulphur dioxide concentrations. *Nature* 366:327–329.
20. Sagan C, Mullen G (1972) Earth and Mars: Evolution of atmospheres and surface temperatures. *Science* 177:52–56.
21. Minton DA, Malhotra R (2007) Assessing the massive young sun hypothesis to solve the warm young earth puzzle. *Astrophys J* 660:1700–1706.
22. Sagan C, Chyba CF (1997) The early faint sun paradox: Organic shielding of ultraviolet-labile greenhouse gases. *Science* 276:1217–1221.
23. Owen T, Cess RD, Ramanathan V (1979) Early Earth: An enhanced carbon dioxide greenhouse to compensate for reduced solar luminosity. *Nature* 277:640–642.
24. Catling DC, Claire MW (2005) How Earth's atmosphere evolved to an oxic state: A status report. *Earth Planet Sci Lett* 237:1–20.
25. Rye R, Kuo PH, Holland HD (1995) Atmospheric carbon dioxide concentrations before 2.2 billion years ago. *Nature* 378:603–605.
26. Sheldon ND (2006) Precambrian paleosols and atmospheric CO_2 levels. *Precambrian Res* 147:148–155.
27. Pavlov AA, Brown LL, Kasting JF (2001) UV shielding of NH_3 and O_2 by organic hazes in the Archean atmosphere. *J Geophys Res* 106:23267–23288.
28. Domagal-Goldman SD, Kasting JF, Johnston DT, Farquhar J (2008) Organic haze, glaciations and multiple sulfur isotopes in the Mid-Archean Era. *Earth Planet Sci Lett* 269:29–40.
29. Ueno Y, Yamada K, Yoshida N, Maruyama S, Isozaki Y (2006) Evidence from fluid inclusions for microbial methanogenesis in the early Archaean era. *Nature* 440:516–519.
30. Young GM, Von Brunn V, Gold DJC, Minter WEL (1998) Earth's oldest reported glaciation: Physical and chemical evidence from the Archean Moan Group (~2.9 Ga) of South Africa. *J Geol* 106:523–538.
31. Ohmoto H, Watanabe Y, Ikemi H, Poulson SR, Taylor BE (2006) Sulphur isotope evidence for an oxic Archaean atmosphere. *Nature* 442:908–911.
32. Ono S, Beukes NJ, Rumble D, Fogel ML (2006) Early evolution of atmospheric oxygen from multiple-sulfur and carbon isotope records of the 2.9 Ga Mozaan Group of the Pongola Supergroup, Southern Africa. *South African J Geol* 109:97–108.
33. Farquhar J, et al. (2007) Isotopic evidence for Mesoarchaean anoxia and changing atmospheric sulphur chemistry. *Nature* 449:706–709.
34. Hulston JR, Thode HG (1965) Variations in ^{33}S, ^{34}S and ^{36}S contents of meteorites and their relation to chemical and nuclear effects. *J Geophys Res* 70:3475–3484.
35. Okazaki A, Ebata T, Mikami N (1997) Degenerate four-wave mixing and photofragment yield spectroscopic study of jet-cooled SO_2 in the C^1B_2 state: Internal conversion followed by dissociation in the X state. *J Chem Phys* 107:8752–8758.
36. Rottman GJ, Woods TN, McClintock W (2006) SORCE solar UV irradiance results. *Adv Space Res* 37:201–208.
37. Danielache SO, Nanbu S, Eskebjerg C, Johnson MS, Yoshida N (2009) Carbonyl sulfide isotopologues: Ultraviolet absorption cross sections and stratospheric photolysis. *J Chem Phys* 131:024307.